JOURNAL OF SOLID STATE CHEMISTRY 72, 155–172 (1988)

Potassium Monophosphate Tungsten Bronzes with Hexagonal Tunnels, $K_x(PO_2)_4(WO_3)_{2m}$: X-ray Diffraction and HREM Study

B. DOMENGÈS, M. HERVIEU, AND B. RAVEAU

Laboratoire de Cristallographie et Sciences des Matériaux de l'U.A. 251, ISMRa, Av. du Maréchal Juin, Caen Cedex 14032, France

AND M. O'KEEFFE

Department of Chemistry, Arizona State University, Tempe, Arizona 85287

Received January 21, 1987; in revised form May 20, 1987

The series $K_x(PO_2)_4(WO_3)_{2m}$ has been investigated by X-ray diffraction and electron microscopy. Five compositions have been isolated as pure phases for $x = 2$ and $m = 4, 6, 7, 8$, and 10. These bronzes are built up from WO_3 slabs connected through PO_4 groups forming hexagonal tunnels. High-resolution lattice images allow a correlation between the image contrast and the structure to be established. Three groups of defects are observed in the crystals which deal with (i) the distribution of the phosphate planes with respect to the ReO_3-type slabs, (ii) the distribution of the K^+ ions in the tunnels, and (iii) the uneven arrangements of the phosphate planes. From this study, it appears that the mechanism of nonstoichiometry is different from that observed in the other phosphate tungsten bronze families according to the existence range and the specific defects which generally involve large parts of the bulk.

Introduction

In the course of the investigation of the A–P–W–O systems (A = Na, K, Rb), two families of phosphate tungsten bronzes were isolated, which were formulated $A_x(P_2O_4)_2(WO_3)_{2m}$ and $A_x(PO_2)_4(WO_3)_{2m}$. Those bronzes which have a variable A ion content are called diphosphate tungsten bronzes with hexagonal tunnels ($DPTB_H$) and monophosphate tungsten bronzes with hexagonal tunnels ($MPTB_H$), respectively. Only three members of the $MPTB_H$'s, $A_x(PO_2)_4(WO_3)_{2m}$, have been isolated for A = K and Na and studied by X-ray diffraction up to the present (*1–3*). Previous results have suggested that a study of the problems of stability and nonstoichiometry of these oxides would indeed be of interest. Thus HREM studies of the $DPTB_H$'s have shown the existence of numerous defects and microstructures related to the adaptability of phosphate groups to the WO_3 matrix (*4–7*). In this respect, the HREM investigation of the monophosphate tungsten bronzes with pentagonal tunnels ($MPTB_P$) $(PO_2)_4(WO_3)_{2m}$ (*8, 9*) which showed the existence of microstructures resulting from the recurrent intergrowth of $MPTB_P$'s and $MPTB_H$'s suggests a great flexibility of the $MPTB_H$'s structure. The present paper deals with the systematic study of the potassium monophosphate tungsten bronze series $K_x(PO_2)_4(WO_3)_{2m}$, for different x values and integral

0022-4596/88 $3.00

m values, by X-ray diffraction and HREM in order to understand the possible effects of nonstoichiometry in those oxides.

Experimental

Synthesis

Adequate mixtures of K_2CO_3, $H(NH_4)_2PO_4$, and WO_3 were first heated at 823 K in air, in platinum crucibles in order to decompose the potassium carbonate and the ammonium phosphate. The resulting products were then mixed with the necessary amount of metallic tungsten and heated in evacuated silica ampoules at temperatures ranging from 1173 to 1473 K for several days (4 to 8 days). Samples were then quenched to room temperature.

X-ray Diffraction and Electron Microscopy Analysis

All samples were analyzed by X-ray diffraction using a Guinier de Wolff camera and pure compounds were studied with a power diffractometer (Philips), using Cu$K\alpha$ radiation. The electron microscopy study was performed on three different microscopes: JEOL 100CX, Philips EM400 (both operating at 120 kV), and JEOL 200CX (operating at 200 kV). Both JEOL microscopes, when used for high-resolution work, were equipped with a top-entry goniometer (±10°) and an objective lens with a spherical aberration constant C_s = 0.8 mm (0.7 mm in the 100CX). Lattice images were computed by use of the multislice method (*10*).

X-ray and Electron Diffraction Results

Phase Diagram Investigation

Previous X-ray investigations have shown that $MPTB_H$'s $K_x(PO_2)_4(WO_3)_{2m}$, could only be obtained for $x > 1$; for $x \leq 1$, $DPTB_H$s are synthesized (*1, 2*). Thus this study was carried out for integral m values ranging from $m = 2$ to 20 and x values ranging from 1.5 to 4.

The pseudoternary system presented in Fig. 1 helps one understand the relationships between the different bronzes of the system K–P–W–O. It is clear that the nature of the structure is closely related to the potassium content: the diphosphate tungsten bronzes with pentagonal tunnels ($DPTB_P$) (*11*) and the $MPTB_P$'s are characterized by $x = 0$; the $DPTB_H$'s are located on $x = 1$, whereas the $MPTB_H$'s belong to the line $x = 2$.

The investigation of this system by X-ray and electron diffraction for the temperature range given above leads to the following results:

For $1.5 \leq x < 1.75$, mixtures of $DPTB_H$'s and $MPTB_H$'s were always obtained regardless of the experimental conditions.

For $1.75 \leq x \leq 3$, new members—m = 6, 8, 10–were synthesized in addition to the already known members m = 4 and 7. It is worth pointing out that the members m = 5 and 9 seemed to be critical in the synthesis of the phosphate tungsten bronzes. Indeed, the member m = 5 was observed neither in the $DPTB_H$'s with Ba nor in the $MPTB_P$'s and the member m = 9 was difficult to prepare. Microcrystals of m = 9 could be observed by electron microscopy, but the corresponding preparation appeared to be a mixture of m = 9 and 10. All attempts to synthesize higher members than m = 10, by varying the temperature, were unsuccessful.

For $x > 3$, either mixtures of $MPTB_H$'s and tungsten bronzes K_xWO_3 are obtained when $m \leq 10$ or mixtures of WO_3, K_xWO_3, and $DPTB_H$'s when $m > 10$.

Structural Considerations on the $MPTB_H$'s

The $MPTB_H$ compounds crystallize in a monoclinic cell (Fig. 2) for which theoretical parameters can be easily deduced from the ReO_3-like subcell. Analysis of the orien-

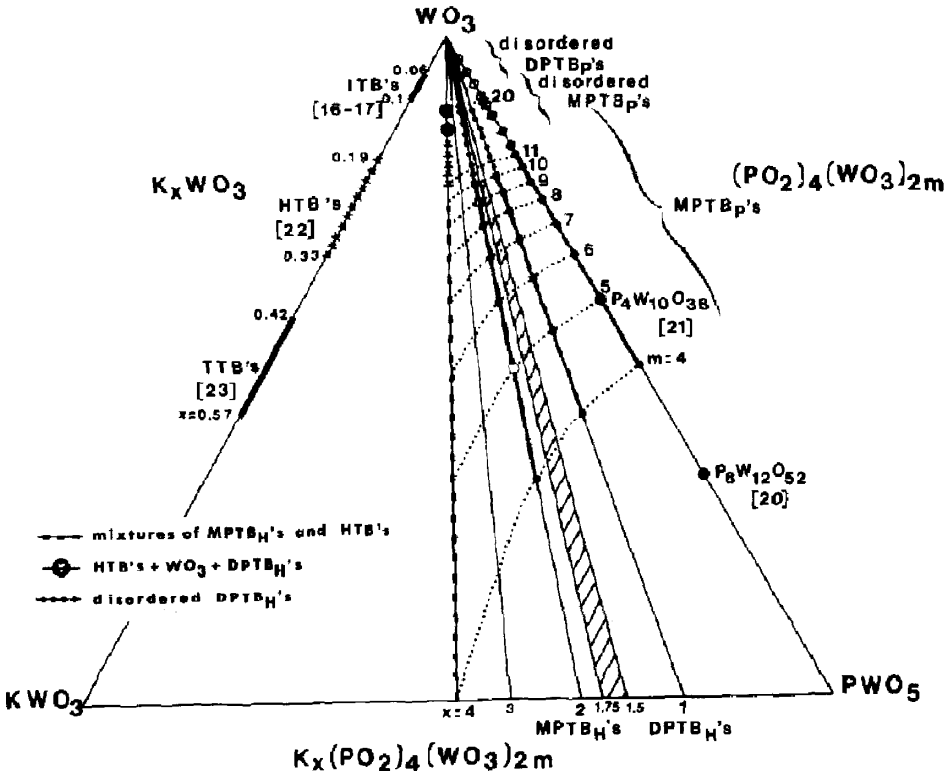

FIG. 1. Pseudoternary KWO_3–PWO_5–WO_3 phase diagram.

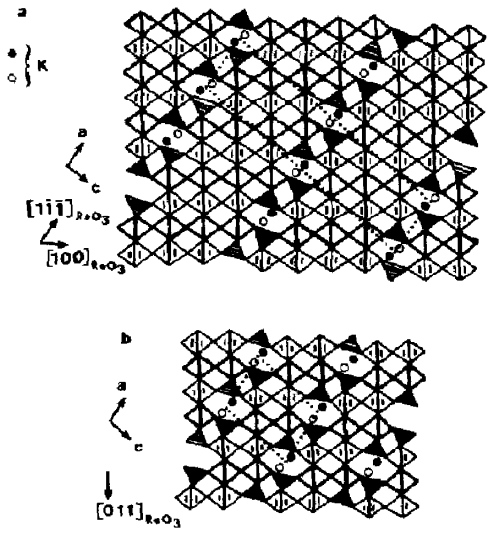

FIG. 2. Projection onto (010) of the idealized structure of (a) $m = 7$ and (b) $m = 4$ members of the series $K(PO_2)_4(WO_3)_{2m}$. Polyhedra with dark and light outlines lie at level $y = \frac{3}{4}$ and $\frac{1}{4}$, respectively.

tation of the PO_4 planes in relation to that of the ReO_3-type slabs has given the following formulas for the odd m values,

$$a_{(th)} = a_R \cdot \sqrt{3}$$

$$b_{(th)} = a_R \cdot \sqrt{2}$$

$$c_{(th)} = \frac{m \cdot a_R \cdot \cos(35.3°) + 2 \cdot K \cdot \cos(16.9°)}{\sin \beta_{(th)}}$$

$$tg\ \beta_{(th)} = \frac{m \cdot a_R \cdot \cos(35.3°) + 2 \cdot K \cdot \cos(16.9°)}{2(a_R\sqrt{3} - K \cdot \sin(16.9°)) - m \cdot a_R \cdot \sin(35.3°)},$$

where $K = 2.56$ Å and m is the number of WO_6 octahedra along the $[011]_R$ direction (R for ReO_3-type matrix). A distinction has to be made between odd m members and even m members. For even m members, c

TABLE I

REFINED PARAMETERS OF THE PREPARED PURE PHASES

m	a (Å)	b (Å)	c (Å)	β(°)	c_{th}	β_{th}
4	6.673(7)	5.327(7)	8.909(7)	100.54(7)	8.8	99.5
6	6.676(4)	5.351(3)	11.867(6)	92.79(5)	11.8	93.7
7	6.677(3)	5.349(3)	26.973(11)	97.24(4)	26.9	97.9
8	6.691(3)	5.343(3)	15.108(8)	100.02(4)	15.1	101.2
10	6.637(3)	5.330(2)	18.455(8)	105.25(4)	18.7	105.9

Note. a_{th} = 6.58 Å, b_{th} = 5.37 Å, m = 4 data used from (*1*).

= $c_{(th)}/2$ corresponds to the width of one WO_3 slab, whereas two slabs form the cell for odd m members (Fig. 2).

The parameters of pure phases have been deduced from the X-ray diffractograms and are in agreement with the theoretical ones (Table I). Space groups identified for the m = 4 and m = 7 members (*1–2*) have been confirmed by electron diffraction for the whole series. Even m-member crystals show the systematic extinction $0k0$, $k = 2n + 1$ in agreement with the $P2_1/m$ space group, whereas the odd m-member compounds, with the systematic extinction hkl $k + l = 2n + 1$ crystallize in the $A2/m$ space group.

HREM Study

Images of the hexagonal tunnels in the monophosphate tungsten bronzes were previously observed as defects in the $MPTB_P$'s (*8*). From these studies, it appeared that the interpretation of the contrast was sometimes not obvious. Moreover the insertion of potassium in the tunnels provides a major source of contrast variations (*12, 13*).

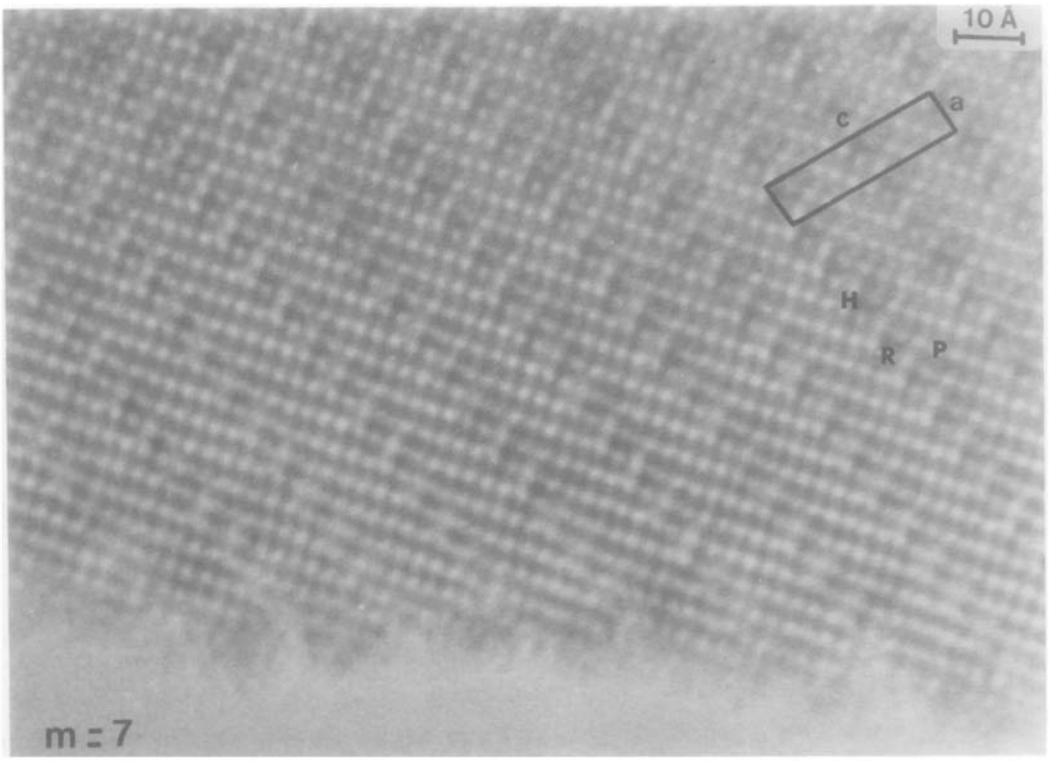

FIG. 3. High-resolution image of an m = 7 microcrystal, projected onto (010). White (H), (P), and (R) dots correspond to the three types of tunnels in the structure: hexagonal, perovskite-type, rhombic (Jeol 200CX).

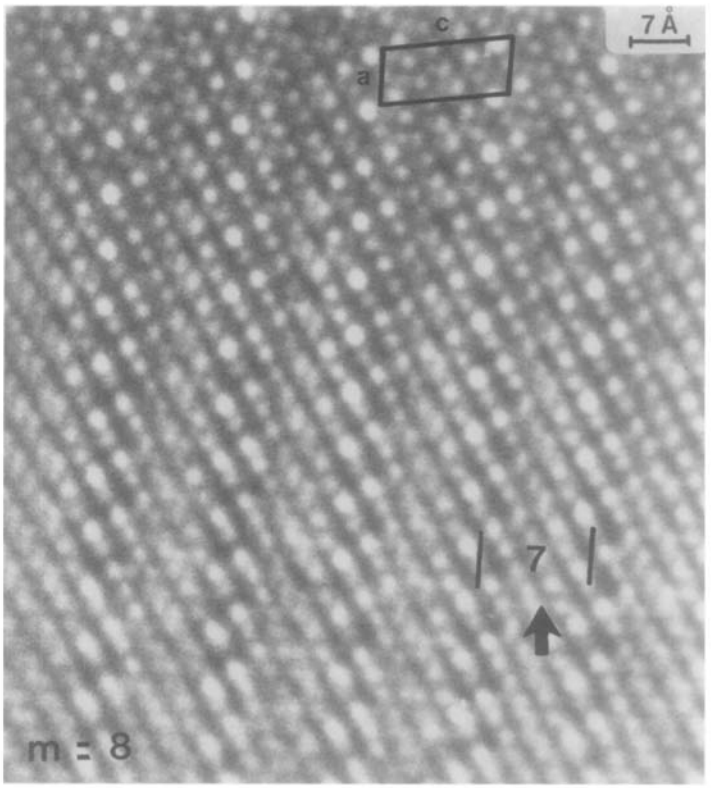

FIG. 4. High-resolution image of an $m = 8$ microcrystal, projected onto (010). An $m = 7$ slab (arrow) appears as a defect in the matrix (Jeol 200CX).

Thus the HREM study of the $MPTB_H$'s was carried out as a first step on regular members in order to interpret the observed images, using image computations; the investigation of deviation from stoichiometry and defects was then undertaken.

Regular Crystals

The first HREM observations were made with the axis of the microscope parallel to [010] in order to confirm the structure of this series. Figures 3 and 4 show typical examples of the observed contrast. On the thin edges of the crystals, white dots can be correlated with the tunnels of the structure. Thus in the WO_3 slabs, dots spaced at 3.8 Å along $[001]_R$ and 2.7 Å along $[110]_R$ can be associated with the perovskite-type tunnels. Along [100], pairs of dots alternate with one dot. They correspond to the hexagonal and rhombic tunnels of the structure, respectively. The splitting in two of the dots corresponding to the hexagonal tunnels is due to the presence of the potassium ions. The identification of each member of the series can be directly made by counting the number of perovskite-type tunnels (six in Fig. 3 and seven in Fig. 4). Calculations have been performed in order to confirm this image interpretation. Figure 5 compares an observed through-focus series to the calculated one for the member $m = 7$, positional parameters being taken from the single crystal X-ray diffraction study (*2*). For a thickness of 32.09 Å and at the optimum defocus −320 Å, the image really shows a direct projection of the

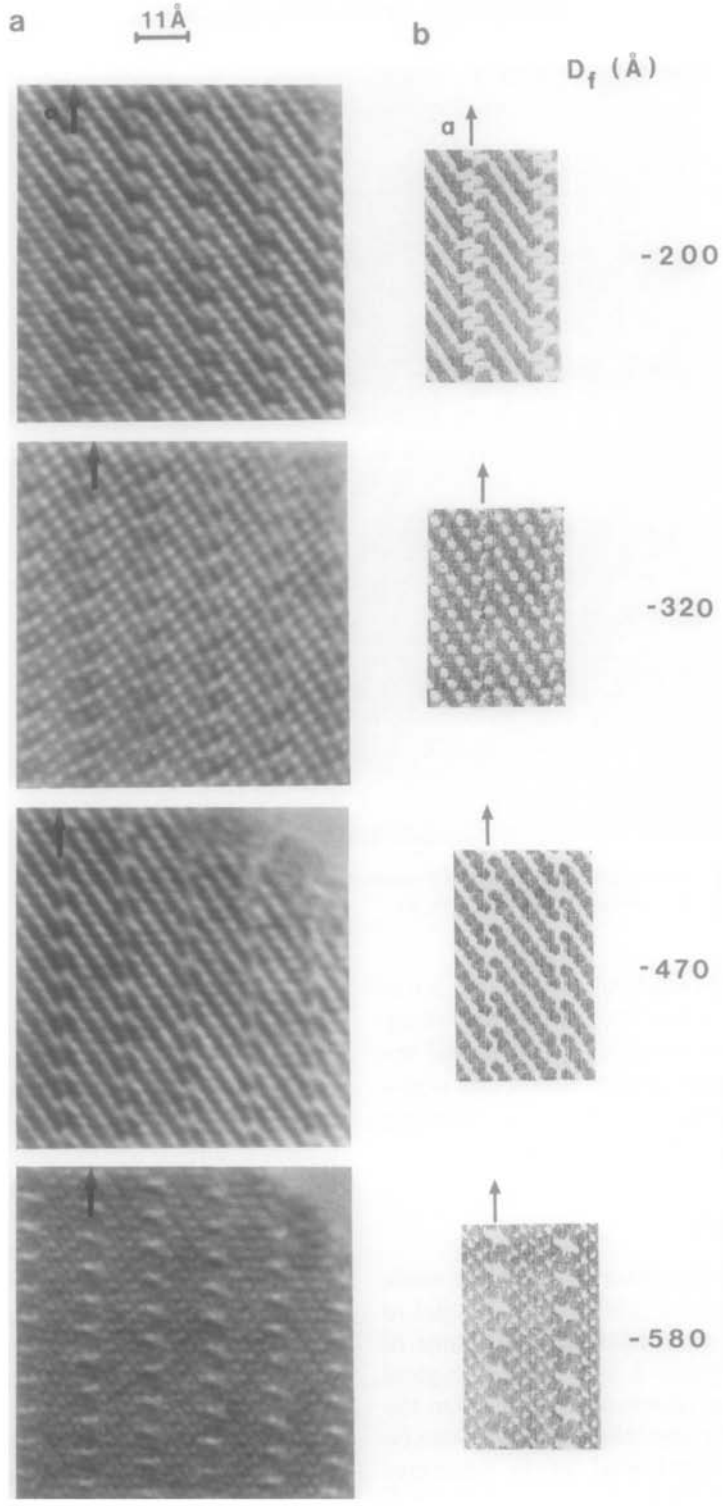

FIG. 5. Through-focus series (a) observed and (b) calculated with the parameters: accelerating voltage = 200 kV, thickness = 32.09 Å, C_s = 0.8 mm, half-divergence angle = 0.8 mrad, 211 beams in the objective aperture.

structure and confirms the intuitive interpretation.

Part of this study has been carried out on a Jeol 100CX. The comparison between the observed images on both microscopes providing two different values of the theoretical resolution (2.75 and 2.2 Å, respectively) was made on regular microcrystals. As expected, perovskite-type tunnels and rhombic tunnels are not so well resolved with the JEM 100CX.

Another direction of observation appeared interesting especially in the study of defects. With the microscope axis parallel to [100], images give a good description of the PO_4 groups stacking along the [010] direction. As deduced from the projection parallel to [100] (Fig. 6) and the resolving power limit of the microscope, the easiest images to interpret would be those where light contrast would correspond to the high electronic density zones of the crystal. This was confirmed by observations and calculations, as shown in Fig. 7. For a defocus value of −700 Å, the high-resolution image of an $m = 7$ microcrystal shows slabs of alternating three and four bright spots corresponding to the W atoms of the structure joined through slightly smaller spots, running in quincunx along [010], which correspond to the P atoms (Fig. 7b). Again the member of the series can be easily identified by counting the number of tungsten atoms in a WO_3 slab.

Observation of Defects

The defects observed in the $MPTB_H$'s can be classified into three groups which deal with (i) the distribution of the phosphate planes with respect to the ReO_3-type slabs, (ii) the distribution of the K^+ ions in the tunnels, and (iii) the distribution of the PO_4 groups in the phosphate planes.

(i) The building principle of the $MPTB_H$'s structure can be compared to that observed in numerous nonstoichiometric oxides: the phosphate planes which connect the ReO_3-type slabs can be compared to the *CS* planes in the tungsten suboxides (*14, 15*) or to the tunnel rows in the ITB family, for instance (*16, 17*). The existence of such planes can lead to intergrowth phenomena or at least to the formation of bidimensional defects in the matrix. This suggests that the possible variation of the width of the ReO_3-type slabs due to a local change in the m value must be considered; in the same way the occurrence of domains due to changes in the direction of the phosphate planes or to the formation of another structural type are possible. The HREM observations of the $MPTB_H$'s confirm this point of view: it appears rather difficult to find a perfectly regular crystal, though the diffraction patterns look perfect. WO_3 slabs corresponding to an m value different from that of the matrix are frequently observed; one example is shown in Fig. 4 where a member $m =$

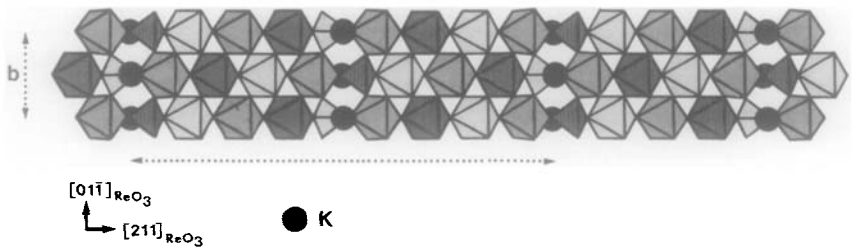

FIG. 6. Projection parallel to [100] of the term $m = 7$. Dotted lines indicate the periodicity.

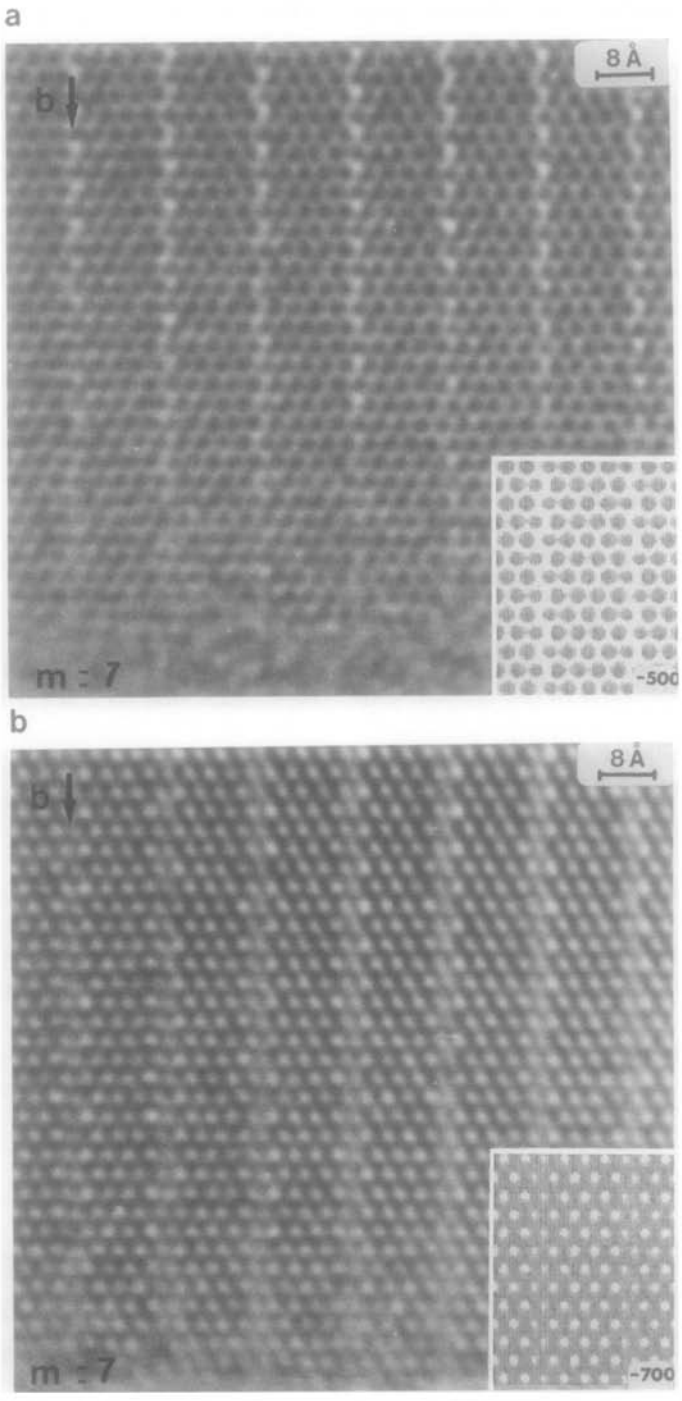

FIG. 7. HREM observed and calculated images of an $m = 7$ microcrystal projected in parallel to [100]. Calculation parameters are accelerating voltage = 200 kV, thickness = 26.64 Å, $C_s = 0.8$ mm, half-divergence angle = 0.8 mrad, 55 beams in the objective aperture, defocus value (a) −500 Å and (b) −700 Å.

7 appears in a matrix $m = 8$. These defects are generally isolated and seldom lead to actual intergrowths; only one intergrowth was observed with the sequence [9 : 10] (Fig. 13).

A new, frequently observed defect was characterized. It corresponds to coherent outgrowth or domains on the edges of the parent crystal. In Fig. 8 the crystal edge looks like a mosaic, yet the diffraction pattern is characteristic of a regular $m = 6$ member (Fig. 8b). This can be explained by the tiny size (≈ 320 nm^2) of the crystallites compared to that of the selected area for the diffraction pattern (area ratio $< 2 \times 10^{-3}$). As a consequence and because of the number of domains, our optical bench could not be used to identify them.

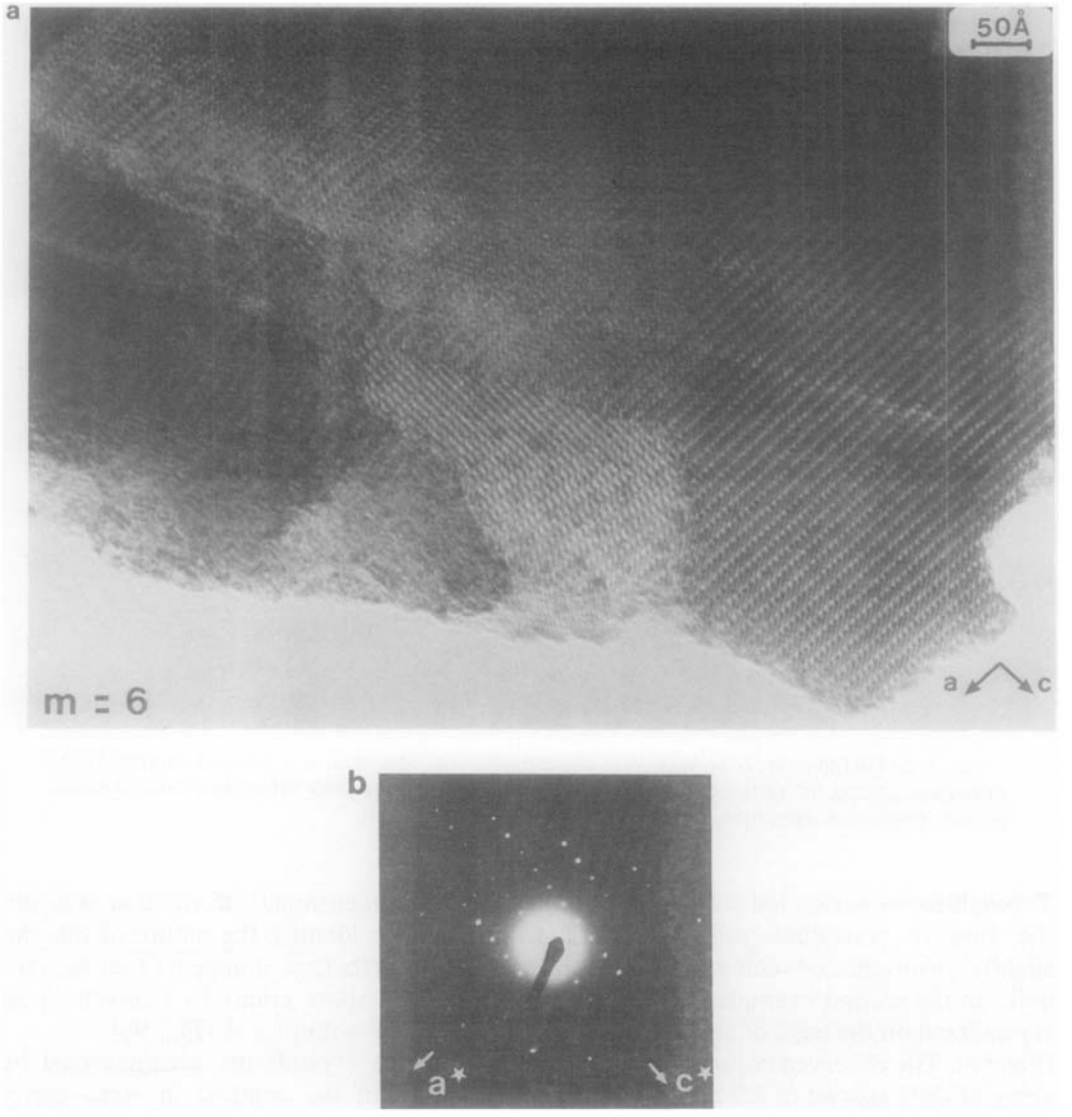

FIG. 8. (a) HREM image of an $m = 6$ microcrystal showing on the edge a mosaic-like contrast (Jeol 100CX). (b) Corresponding diffraction pattern, microscope axis is parallel to [010].

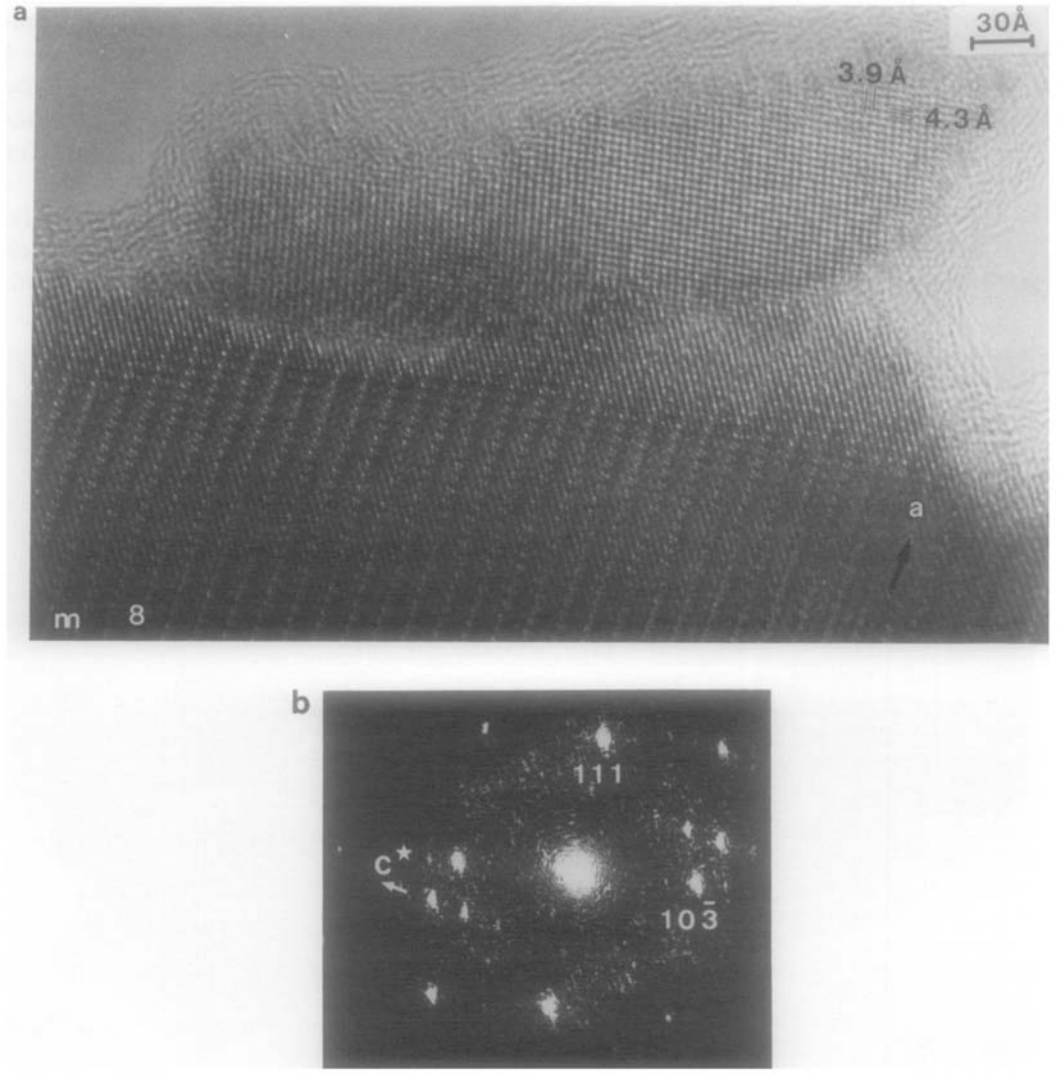

FIG. 9. (a) HREM image of an outgrowth crystallized on the edge of an $m = 8$ crystal, projected onto (010) (Jeol 200CX). (b) Outgrowth optical diffractogram, weak extra spots belong to c^* axis of parent crystal. Outgrowth diffraction pattern can be indexed in $m = 8$ cell.

Through-focus series led us to think that the biggest crystallite was an $MPTB_H$ slightly disorientated compared with the bulk. In the second example, an outgrowth crystallized on the edge of an $m = 8$ crystal (Fig. 9a). The observed contrast is a regular array of dots spaced at 3.9 and 4.3 Å with an angle of 96°. These parameters have been confirmed by an optical diffractogram: this two-dimensional information was not sufficient to identify the nature of this domain; nevertheless, it appears that the corresponding spots could be indexed in an $MPTB_H$ cell with $m = 8$ (Fig. 9b).

(ii) Some crystals are characterized by anomalies of the contrast in areas corresponding to the hexagonal tunnels; their diffraction patterns then exhibit extra spots

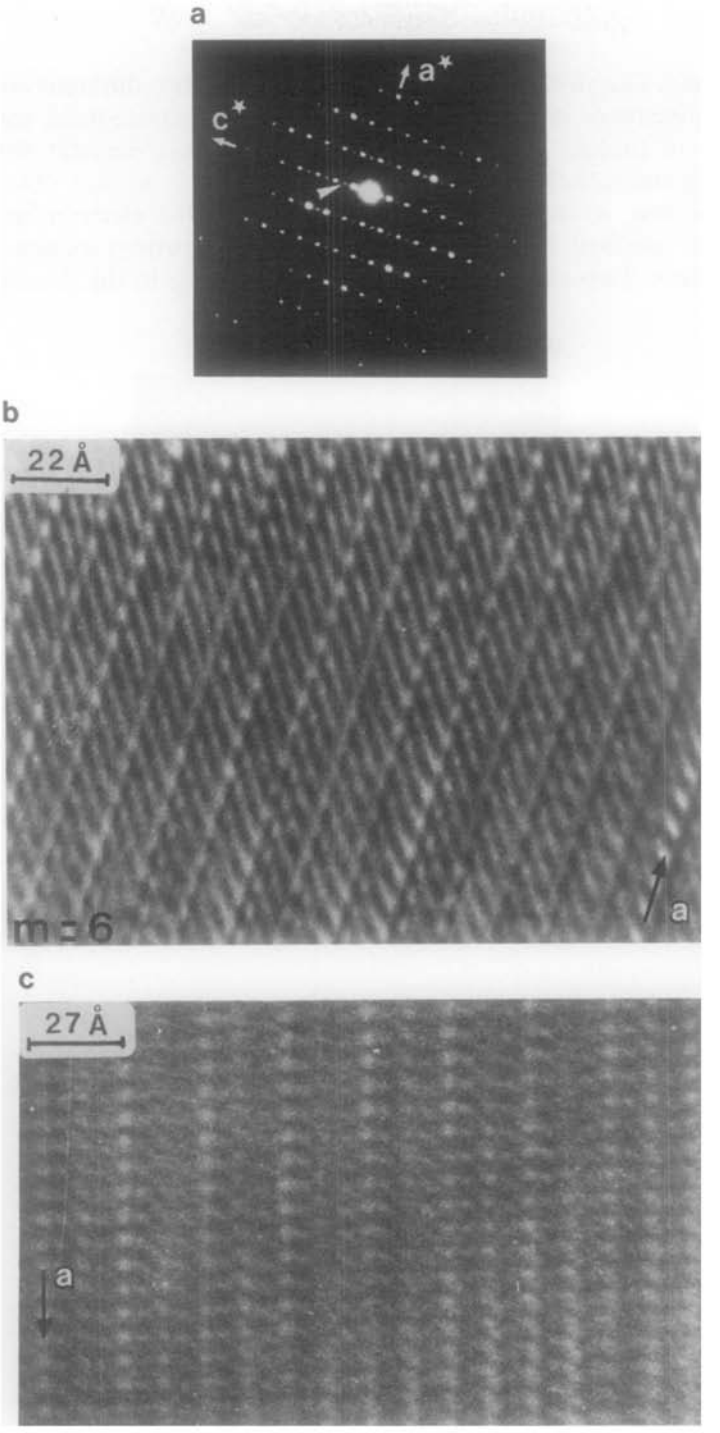

FIG. 10. (a) An $h0l$ diffraction pattern of an $m = 6$ crystal showing superstructure spots (arrow) involving the doubling of the c parameter. Corresponding images (Jeol 100CX), (b) medium resolution showing contrast variation in the rows of spots associated with hexagonal tunnels of the structure, (c) thicker region of the crystal, where one hexagonal tunnel row out of two is systematically darkened, suggest a variation of K occupation ratio in the hexagonal tunnels.

or diffuse streaks. The variation of the contrast appears sometimes in a random way, from one row of tunnels to the other or from one hexagonal tunnel to the adjacent one in the same row, so that the phenomenon cannot be ascribed to variations of thickness or focus. Two examples, corresponding to two different orientations of the crystals, illustrate these features.

The first microcrystal, with nominal composition $m = 6$, was observed with [010] parallel to the electron beam; its electron diffraction pattern exhibits superstructure spots leading to the doubling of the c pa-

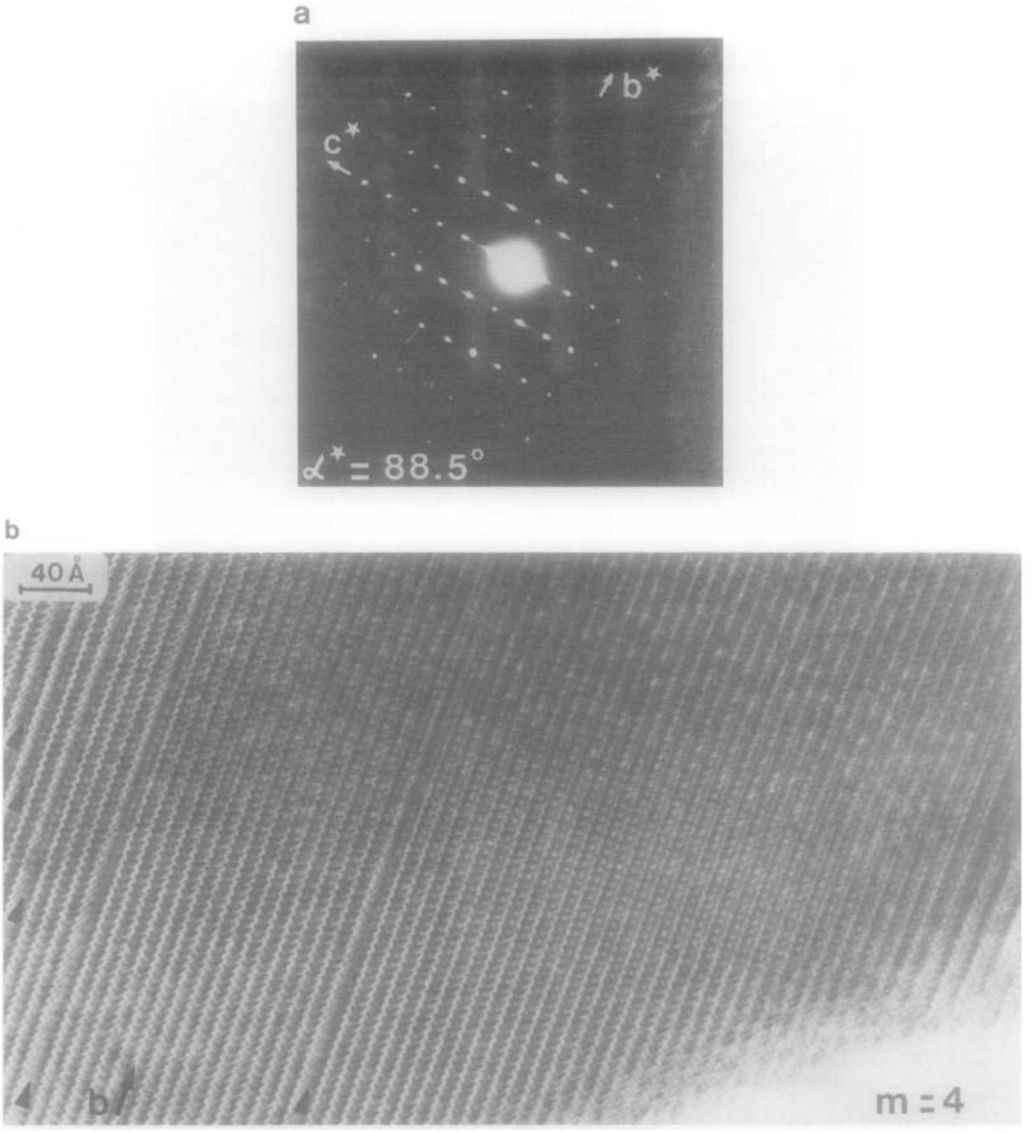

FIG. 11. (a) A $0kl$ diffraction pattern of a crystal with a mean term $m = 4$. The triclinic deformation is measured by $\alpha = 91.5°$. Diffuse streaks lie along [001]*. (b) Corresponding HREM image with five $m = 6$ slabs and speckled contrast in the thick region associated with a variation of K occupation ratio in hexagonal tunnels (Jeol 100CX).

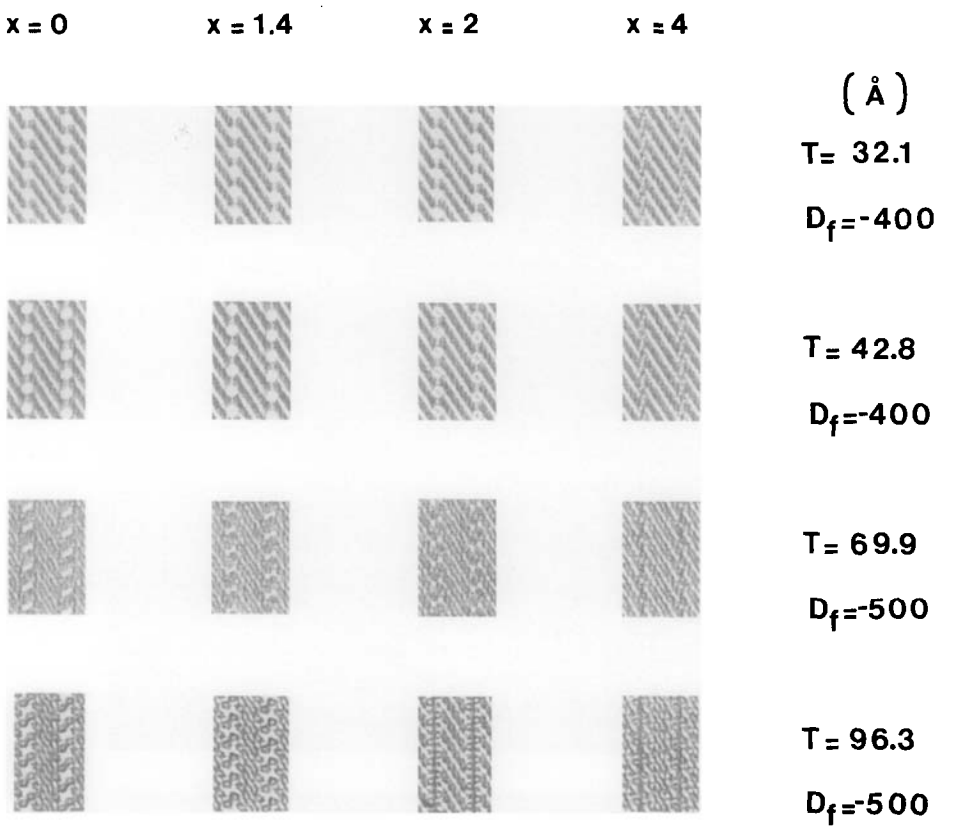

FIG. 12. (010) Calculated images for different K occupation ratio x and thicknesses T, with the following parameters: accelerating voltage = 120 kV, C_s = 0.7 mm, half-divergence angle = 0.65 mrad, and 49 beams in the objective aperture.

rameter (Fig. 10a); these extra spots are slightly extended along c^*. Corresponding images are shown in Figs. 10b and 10c. In Fig. 10b, variations of the contrast of the tunnel rows are obvious close to the crystal edge, from one row to the other and even along a row; in a thicker part of the crystal, Fig. 10c, one row out of two systematically appears darker (related to the doubling of the c parameter).

The diffraction pattern of the second example was taken with the electron beam parallel to [100] (Fig. 11a). It is characterized, this time, by diffuse streaks parallel to [001]* and a triclinic deformation. Nevertheless the mean member could be identified as $m = 4$. The phosphate planes appear as zigzag bright rows parallel to [010] in the HREM image where five $m = 6$ slabs are observed (Fig. 11b). The thicker regions of the image are characterized by a speckled contrast.

Such variations of the tunnel contrast which are clearly observed in crystal bulk and systematically imply extra spots on the ED strongly suggest a more or less ordered variation of potassium distribution in the hexagonal tunnels. Simulated images were calculated for different compositions [x = 1.4 (nominal composition), $x = 2$, $x = 4$ (fully occupied tunnels), and $x = 0$ (empty tunnels)], for different thickness values (T), and for both observation orientations. Some [010] calculated images are shown in

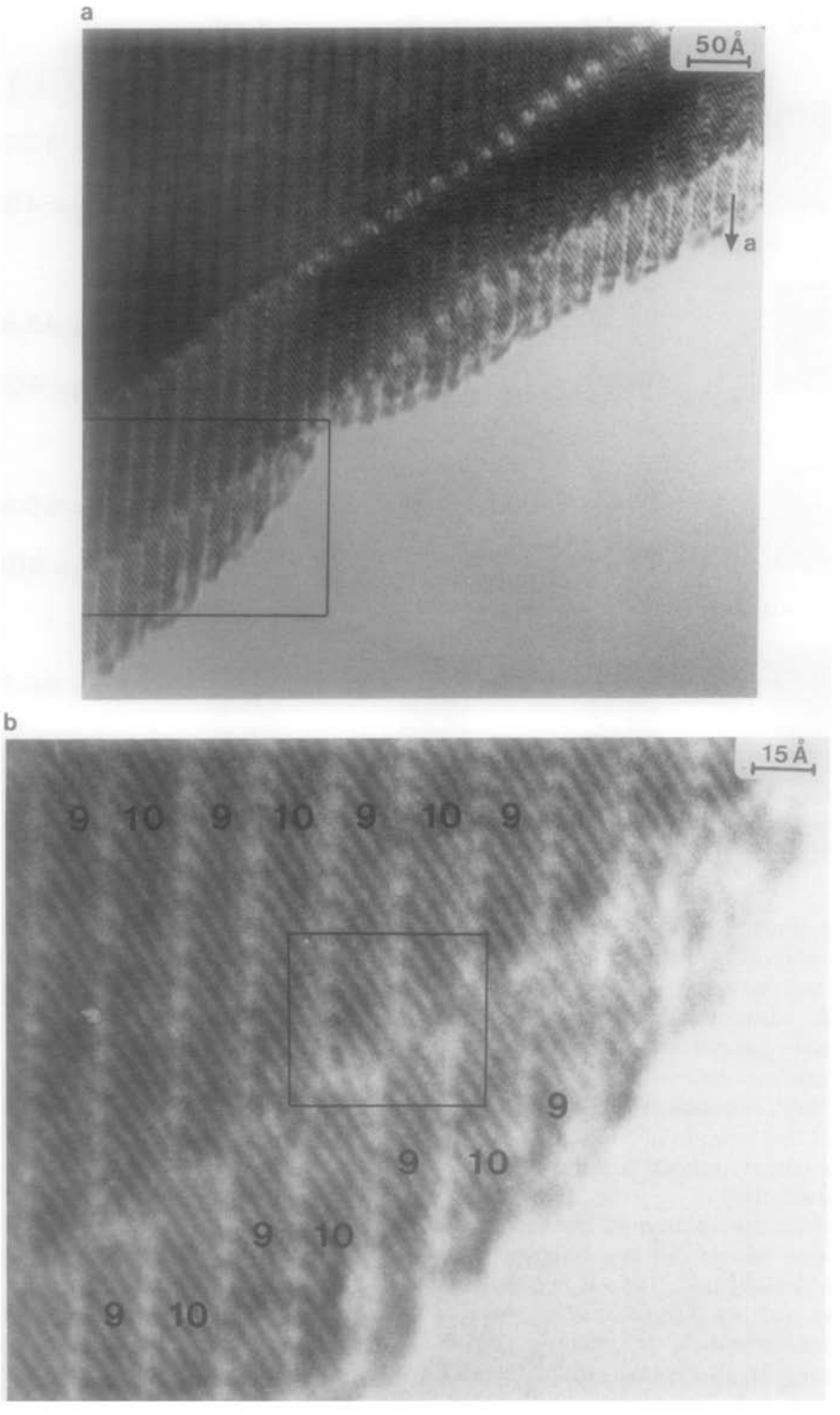
a
50 Å
a
b
15 Å
9 10 9 10 9 10 9
9
9 10
9 10
9 10

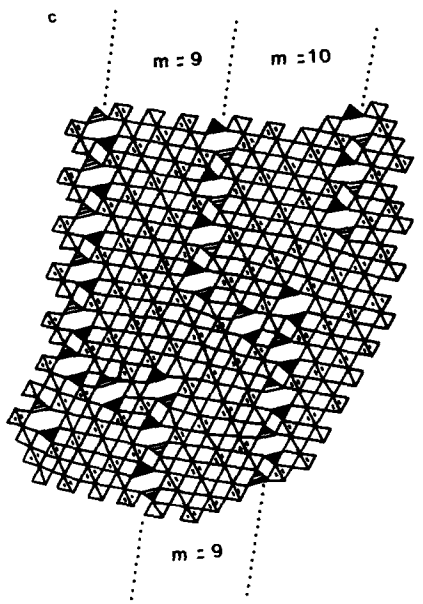

FIG. 13. (a) Medium resolution image of an $m = 10$ microcrystal projected onto (010) (Philips EM400). Nearly each row of brighter spots corresponding to hexagonal tunnels stops and shifts. (b) Enlarged detail shows that WO_3 slab width is the same on each side of the PO_4 row shifting: regular intergrowth $|m = 9 : m = 10|$. (c) Idealized projection onto (010) of the proposed model for the outlined defect zone in (b).

Fig. 12. They confirm, only in a qualitative way indeed, the interpretation of the contrast variations as a witness of the potassium occupation variations.

(iii) Shifting and stopping of the tunnel rows is a characteristic feature of potassium diphosphate tungsten bronzes, $DPTB_H$'s (*5–6*); they were also often observed in the empty hexagonal tunnel rows intergrown with the $MPTB_P$'s (*8*). Such a type of defect was then obviously expected in the $MPTB_H$'s. As a matter of fact, they arise rather rarely and then appear more as growth defects involving the whole matrix than as isolated ones. Figure 13a is a medium resolution image of an $m = 10$ crystal. Rows of big gray dots can be associated with hexagonal tunnels and gray streaks with the perovskite-type tunnels. Nearly each phosphate row stops and most of them go on after a translation of several angstroms. The accommodation of this growth defect depends on a basic principle of the phosphate tungsten bronzes, i.e., the easy adaptability of the PO_4 tetrahedra to the WO_6 octahedra. In the enlarged detail, the defect zone is identified as a regular intergrowth $|m = 9 : m = 10|$ (Fig. 13b). Stopping and shifting of phosphate rows are explained by replacement of a column of PO_4 tetrahedra by a column of WO_6 octahedra, in the same way as they are in the defect previously observed in the $MPTB_P$'s (*9*). As seen on the proposed model in Fig. 13c, it only involves slight deformations of the surrounding WO_3 framework.

The next example was observed on an $m = 7$ crystal with the electron beam parallel to [100] (Fig. 14a). On the crystal edge, shifting of several consecutive PO_4 rows is observed, implying a slight disorientation of the $MPTB_H$ matrix on each side of the line of defects. This defect is associated with the local stacking, along the *b* direc-

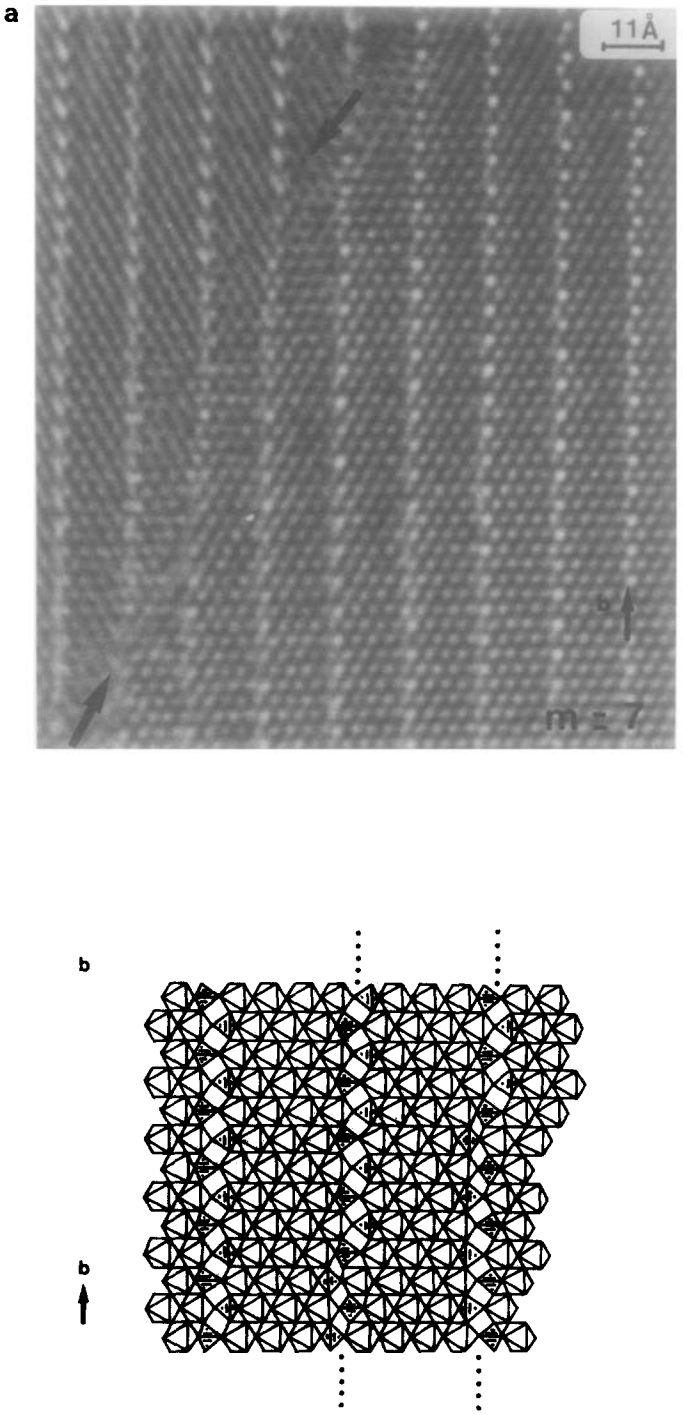

FIG. 14. (a) High-resolution image of an $m = 7$ crystal projected along [100]. Along the fracture on the edge of the crystal (arrows), PO_4 rows shift. (b) Proposed model for the shifting; PO_4 tetrahedra are hatched.

tion, of slabs exhibiting a width different from $m = 7$. The junction between these slabs through PO_4 groups and WO_6 octahedra is not obvious and several models, more or less complex, could be proposed to explain the accommodation of the defect. The easiest is proposed in Fig. 14b, which implies the presence, in the octahedra of the junction, of an unshared oxygen; such an association of PO_4 groups with MO_6 octahedra exhibiting an unshared oxygen were previously observed in $P_2W_2O_{11}$ (*18*) or phosphomolybdate (*19*).

Discussion

From this study, the main structural features of the $MPTB_H$'s have been characterized and comparison with the other PTB's revealed some peculiarities which are worth outlining:

- The $m = 5$ member appears as an exception, as in the monophosphate tungsten bronzes with pentagonal tunnels. It seems that the stress imposed by the junction of uneven short rows of octahedra (two and three octahedra) through PO_4 groups destabilizes the host lattice. Moreover, the phenomenon is enhanced in the $MPTB_H$'s for we never observed a five-octahedron-wide slab, even stabilized as an isolated defect, contrary to the other family.
- In the same way, the upper limit of the existence range is remarkable, in the systematic nonexistence of WO_3 slabs wider than 10 octahedra. This feature appears even more amazing as the appearance of broad slabs, sometimes extending to WO_3 domains, is a typical behavior not only of the PTB's but also of other phases characterized by the same building principles such as ITB's or *CS* phases.
- The major part of the observed defects, except those previously mentioned about the WO_3 slab width (i.e., outgrowth, ordering of the potassium ions, and shifting of the PO_4 groups), occurs generally in an extended area of the microcrystals; this is unusual in the phosphate bronze families where the adaptability of the PO_4 groups to the WO_3 framework leads to numerous isolated defects.

Conclusion

Thus, from these results, it clearly appears that $MPTB_H$'s exhibit an original structural behavior which could not be expected from the plain consideration of the host lattice. It is now necessary to determine the role of the A ion nature in such phenomena. The study of the $MPTB_H$'s involving smaller A ions such as sodium in the hexagonal tunnels may bring a partial answer.

Acknowledgment

A major part of this work was supported by a grant from the National Science Foundation (DMR 84-18083).

References

1. J. P. Giroult, M. Goreaud, Ph. Labbé, and B. Raveau, *J. Solid State Chem.* **44,** 407 (1982).
2. B. Domengès, M. Goreaud, Ph. Labbé, and B. Raveau, *J. Solid State Chem.* **50,** 173 (1983).
3. A. Benmoussa, D. Groult, Ph. Labbé, and B. Raveau, *Acta Crystallogr. C* **40,** 573 (1984).
4. M. Hervieu and B. Raveau, *J. Solid State Chem.* **43,** 299 (1982).
5. M. Hervieu and B. Raveau, *Chem. Scr.* **22,** 117 (1983).
6. M. Hervieu and B. Raveau, *Chem. Scr.* **22,** 123 (1983).
7. M. Hervieu, B. Domengès, and B. Raveau, *Chem. Scr.* **25,** 361 (1985).
8. B. Domengès, M. Hervieu, R. J. D. Tilley, and B. Raveau, *J. Solid State Chem.* **54,** 10 (1984).
9. B. Domengès, M. Hervieu, and B. Raveau, *Acta Crystallogr. B* **40,** 249 (1984).
10. A. J. Skarnulis, E. Summerville, and L. Eyring, *J. Solid State Chem.* **23,** 59 (1978).
11. M. Hervieu, B. Domengès, and B. Raveau, *J. Solid State Chem.* **58,** 233 (1985).

12. L. A. BURSILL AND G. GRZINIC, *Acta Crystallogr. B* **36,** 2902 (1980).
13. M. HUTCHISON, G. R. AUSTIS, AND R. J. D. TILLEY, *Electron Microsc.* **2,** 57 (1982).
14. B. BLOMBERG, L. KIHLBORG, AND A. MAGNELI, *Arkiv. Kemi* **6,** No. 11, 133 (1953).
15. A. MAGNELI, *Acta Crystallogr.* **6,** 495 (1953).
16. A. HUSSAIN AND L. KIHLBORG, *Acta Crystallogr. A* **32,** 551 (1976).
17. L. KIHLBORG, *Chem. Scr.* **14,** 187 (1978).
18. P. KIERKEGAARD AND S. ASBRINK, *Acta Chem. Scand.* **18,** 2329 (1964).
19. A. LECLAIRE, J. C. MONIER, AND B. RAVEAU, *J. Solid State Chem.* **48,** 147 (1983).
20. B. DOMENGÈS, M. GOREAUD, PH. LABBÉ, AND B. RAVEAU, *Acta Crystallogr. B* **38,** 1724 (1982).
21. A. BENMOUSSA, PH. LABBÉ, D. GROULT, AND B. RAVEAU, *J. Solid State Chem.* **44,** 318 (1982).
22. E. BANKS AND A. GOLDSTEIN, *Inorg. Chem.* **7,** 966 (1968).
23. J. M. RÉAU, C. FOUASSIER, G. LEFLEM, J. Y. BARRAUD, J. P. DOUMERC, AND P. HAGENMÜLLER, *Rev. Chim. Mineral.* **7,** 975 (1970).